Supporting Information

Sorbic Acid as a Triplet Probe: Triplet Energy and Reactivity with Triplet-State Dissolved Organic Matter via $^1O_2$ Phosphorescence

Kyle J. Moor, Markus Schmitt, Paul R. Erickson, and Kristopher McNeill*

Institute of Biogeochemistry and Pollutant Dynamics (IBP), Department of Environmental Systems Science, ETH Zurich, 8092 Zurich, Switzerland

Pages: 35

Figures: 31

Tables: 4

Table of Contents

Section 1. $^1O_2$ Phosphorescence Data Fitting Procedures

Global Kinetic Fitting Approach

Following methodology outlined in a previous report, time-resolved $^1O_2$ phosphorescence traces were fit with an equation that describes $^1O_2$ growth and decay kinetics, essentially a parameterized biexponential growth and decay function, which is governed by the kinetic processes that affect ^{3}CDOM* and $^1O_2$ (eq. S1).[1]

$$[S]_t = \frac{A_0 k_{O_2}[O_2]}{k_d^{\Delta} - k_{HDA}[HDA] - k_d^T - k_{O_2}[O_2]} \left[e^{-(k_{O_2}[O_2] + k_{HDA}[HDA] + k_d^T)t} - e^{-(k_d^{\Delta})t} \right] \quad \text{S1}$$

Rate constants are described in Figure 2a and in the kinetic analysis discussion of the main report. A_0 is the scaling parameter that accounts for instrumental response and $^1O_2$ yields from excited triplet states.

$$A_0 = \kappa k_r^{\Delta} f_{\Delta} [\,^3CDOM^*]_0 \quad \text{S2}$$

where κ is an instrument response factor, k_r^{Δ} is the $^1O_2$ radiative emission rate, f_{Δ} is the fraction of O_2 quenching events that produce $^1O_2$, and [^{3}CDOM*]$_0$ is the initial concentration of ^{3}CDOM*. An identical kinetic scheme is valid for model triplet sensitizers. As discussed in the main report, the quenching of $^1O_2$ by HDA (k_{HDA}^{Δ}) is negligible compared to $^1O_2$ loss by non-radiative relaxation (k_d^{Δ}) and is thus omitted from eq. S1.

The overall fitting approach consisted of simultaneously solving for A_0, which was shared among the different kinetic traces, and k_{HDA} using the input of rate constants that varied depending on the sensitizer. An exception is k_d^{Δ}, which was fixed at 2.76 $\times 10^5$ s^{-1} for all sensitizers.[2] Generally, k_d^T values were used from the literature[1, 3, 4] and $k_{O_2}[O_2]$ values were

46 determined by fitting the $^1O_2$ kinetic trace at [HDA] = 0. For CDOM, an average k_d^T value of
47 9×10^4 s^{-1} was used based on a previous report.[1] Table S1 displays the rate constants used for
48 each sensitizer.
49

Table S1 Rate constants used in global kinetic fits for various sensitizers.

Sensitizer	k_d^T (10^4 s^{-1})	$k_{O_2}[O_2]$ (10^6 s^{-1})
PN	1.3	2.39
CBBP	6.45	1.88
CBBP/PN	3.88	2.24
CDOM	9.0	1.14-1.98

50

51 *Inverse First Order Fitting Approach*

52 An equation was developed to calculate unquenchable fractions of the $^1O_2$
53 phosphorescence and quenching rate constants of triplets by HDA. Integrating the $^1O_2$
54 phosphorescence signal (eq. S1) yields the area of the $^1O_2$ signal, which includes the scaling
55 parameter A_0 (eq. S3):
56

57 $$Area = \frac{A_0 k_{O_2}[O_2]}{(k_{O_2}[O_2]+k_d^T+k_{HDA}[HDA])(k_d^\Delta)} \quad \text{S3}$$

58

59 Normalizing the $^1O_2$ phosphorescence area (S) at a given HDA concentration by the $^1O_2$
60 phosphorescence area at [HDA] = 0 (S_0) yields eq. S4, an inverse first-order equation, which
61 includes a factor b, which is the ratio of triplet quenching by HDA to other loss pathways (eq.
62 S5):
63

64 $$\frac{S}{S_0} = \frac{1-\alpha}{1+b[HDA]} + \alpha \quad \text{S4}$$

$$b = \frac{k_{HDA}}{k_d^T + k_{O_2}[O_2]} \quad \text{S5}$$

where α represents the fraction of triplets that are not quenched by HDA. Experimentally collected $^1O_2$ phosphorescence signals were integrated, yielding areas, normalized to the $^1O_2$ phosphorescence area at [HDA] = 0, and fit with eq. S4. For CDOM and the CBBP/PN validation mixture, $^1O_2$ phosphorescence traces were fit with a generalized form of eq. S1, essentially a generic growth and decay biexponential equation (eq. S6), and the resulting fitted curve was used for integration.

$$[S]_t = \frac{A_0 k_{form}}{k_{decay} - k_{form}} \left(e^{-k_{form}t} - e^{-k_{decay}t}\right) \quad \text{S6}$$

where k_{form} and k_{decay} are the $^1O_2$ phosphorescence signal growth and decay rate constants, respectively. For CBBP/PN experiments, a non-normalized form of eq. S4 was used (eq. S7):

$$S = \frac{(1-\alpha)S_0}{1+b[HDA]} + \alpha S_0 \quad \text{S7}$$

with the same parameters as described in the main report. Quenching rate constants of triplets by HDA were calculated by multiplying the fit term b by the initial growth rate constant of $^1O_2$ phosphorescence at [HDA] = 0, which kinetically is $k_d^T + k_{O_2}[O_2]$.

Section 2. Low-Temperature Phosphorescence

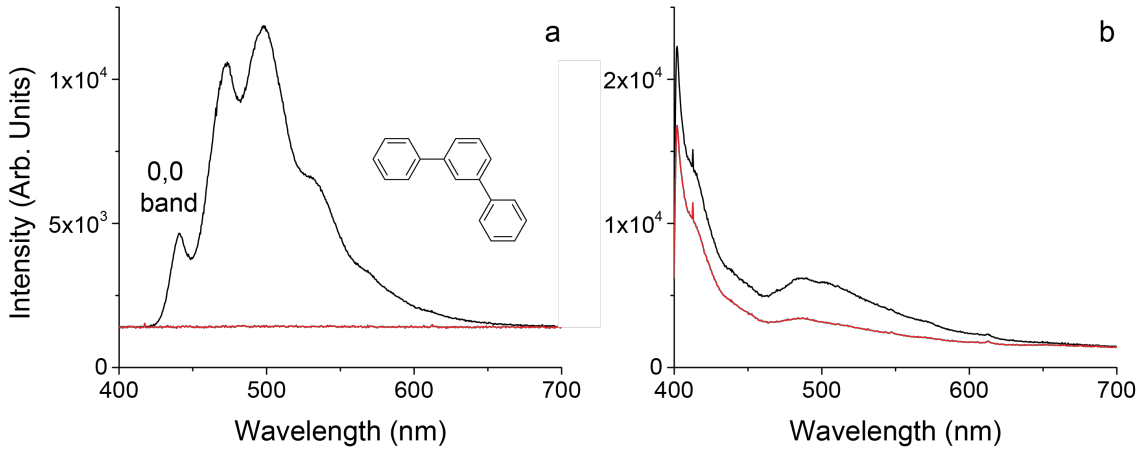

Figure S1 Low temperature phosphorescence emission spectra for (a) m-terphenyl and (b) EPA solvent blank at 77 (black) and 100 K (red).

Section 3. Transient Absorption Measurements

Table S2 Transient absorption spectroscopy experimental details used for measuring quenching rate constants of sensitizer triplets by HDA. Bimolecular rate constants are $\times 10^9$ M^{-1} s^{-1} unless otherwise specified.

Sensitizer	Triplet Energy (kJ mol^{-1})[5, 6]	Excitation λ (nm)	λ transient observed (nm)	k_{HDA}
3-Methoxyacetophenone	303	328	433; 438; 444	2.89 (±0.10)
4-Benzoylbenzoic acid	286	305	532; 542; 552	1.93 (±0.04)
2-Acetonaphthone	249	328	430; 438; 444	3.15 (±0.12)
Riboflavin	209	450	681; 710; 728	0.12 (±0.01)
Perinaphthenone	186	380	476; 481; 486	5.3 (±0.6) $\times 10^6$
Rose Bengal	171	552	601; 604; 610	1.8 (±0.3) $\times 10^5$

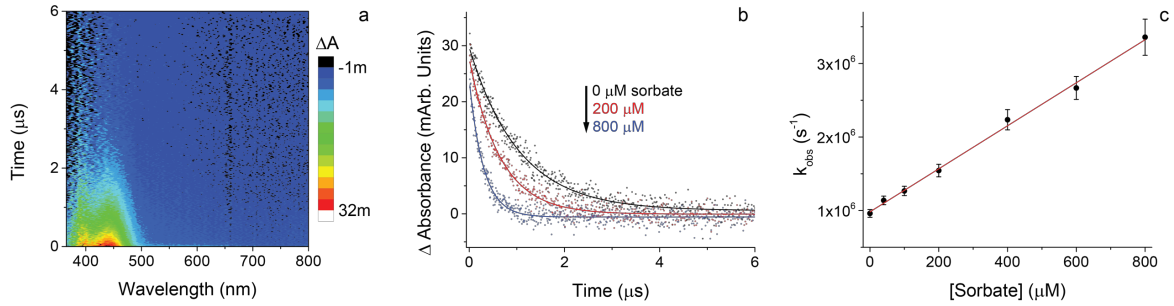

Figure S2 (a) 3-D transient absorption spectrum for ^{3}3MAP* at [HDA] = 0. (b) Kinetic traces for ^{3}3MAP* transient decay monitored at 440 nm under 20% O_2-purged conditions with increasing amounts of HDA. (c) Stern-Volmer plot displaying ^{3}3MAP* decay rate constant as a function of added HDA quencher determined from ^{3}3MAP* transient decay monitored at 440 nm (data presented in b).

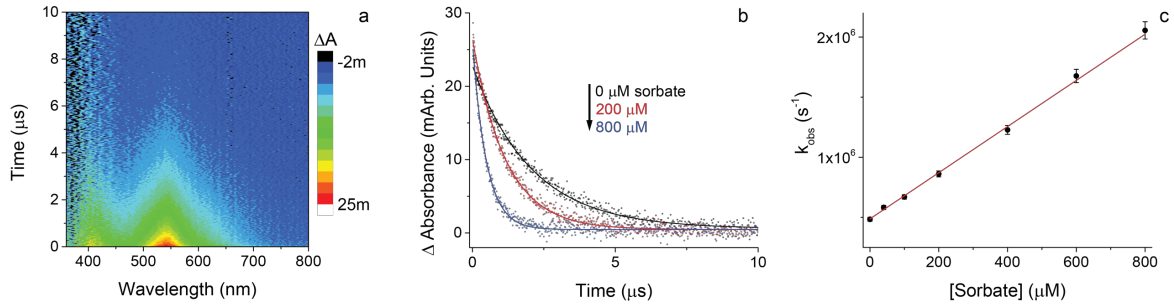

Figure S3 (a) 3-D transient absorption spectrum for ^{3}CBBP* at [HDA] = 0. (b) Kinetic traces for ^{3}CBBP* transient decay monitored at 542 nm under 20% O_2-purged conditions with increasing amounts of HDA. (c) Stern-Volmer plot displaying ^{3}CBBP* decay rate constant as a function of added HDA quencher determined from ^{3}CBBP* transient decay monitored at 542 nm (data presented in b).

97

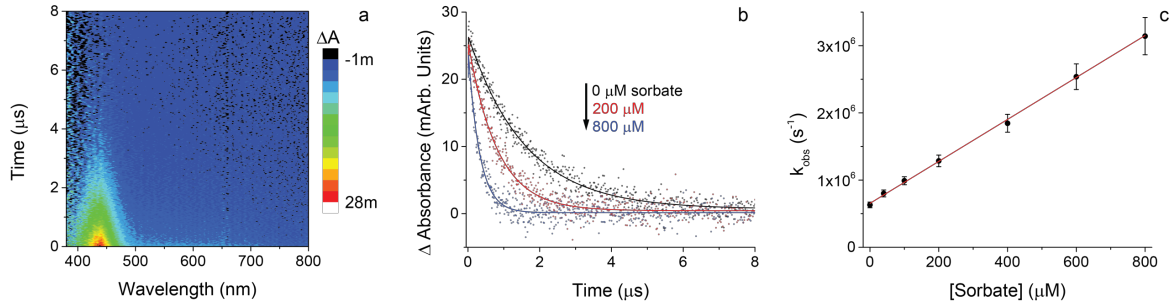

Figure S4 (a) 3-D transient absorption spectrum for ^{3}2AN* at [HDA] = 0. (b) Kinetic traces for ^{3}2AN* transient decay monitored at 438 nm under 20% O_2-purged conditions with increasing amounts of HDA. (c) Stern-Volmer plot displaying ^{3}2AN* decay rate constant as a function of added HDA quencher determined from ^{3}2AN* transient decay monitored at 438 nm (data presented in b).

98

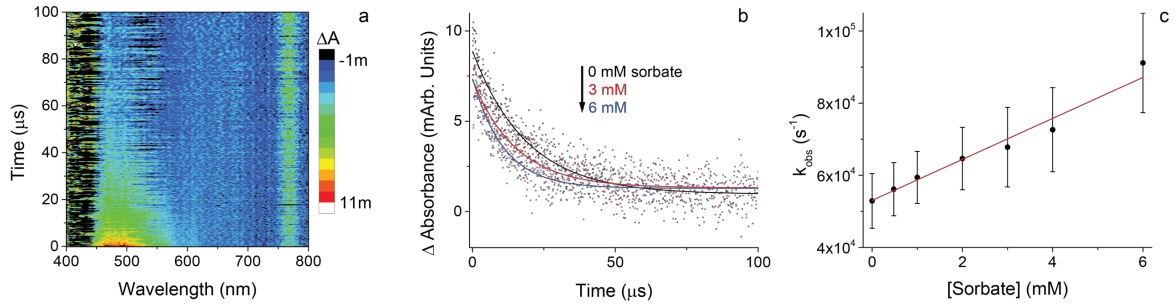

Figure S5 (a) 3-D transient absorption spectrum for ^{3}PN* at [HDA] = 0. (b) Kinetic traces for ^{3}PN* transient decay monitored at 486 nm under N_2O-purged conditions with increasing amounts of HDA. (c) Stern-Volmer plot displaying ^{3}PN* decay rate constant as a function of added HDA quencher determined from ^{3}PN* transient decay monitored at 486 nm (data presented in b).

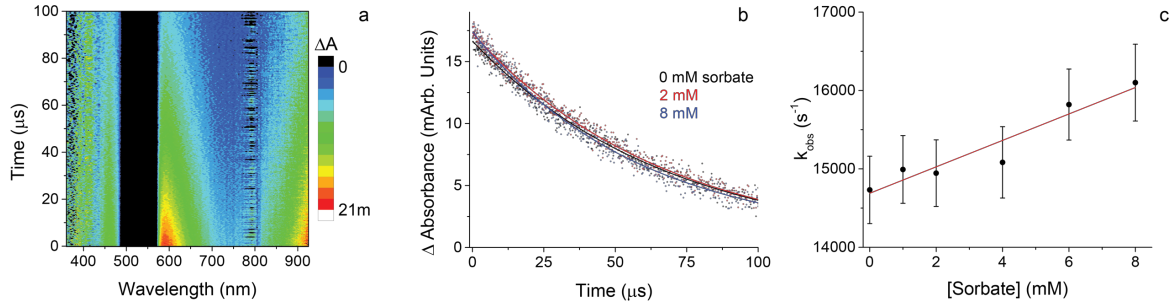

Figure S6 (a) 3-D transient absorption spectrum for ^{3}RB* at [HDA] = 0. (b) Kinetic traces for ^{3}RB* transient decay monitored at 601 nm under Ar-purged conditions with increasing amounts of HDA. (c) Stern-Volmer plot displaying ^{3}RB* decay rate constant as a function of added HDA quencher determined from ^{3}RB* transient decay monitored at 601 nm (data presented in b).

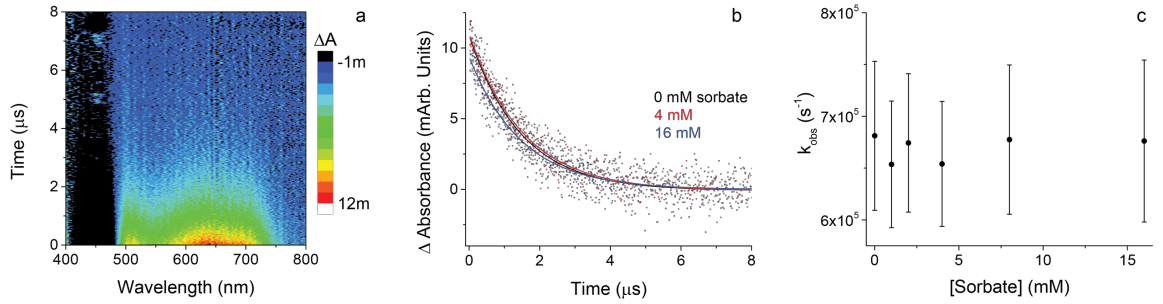

Figure S7 (a) 3-D transient absorption spectrum for ^{3}riboflavin* in methanol at [HDA] = 0. (b) Kinetic traces for ^{3}riboflavin* transient decay monitored at 650 nm under 5% O_2-purged conditions with increasing amounts of HDA. (c) Stern-Volmer plot displaying ^{3}riboflavin* decay rate constant as a function of added HDA quencher determined from ^{3}riboflavin* transient decay monitored at 650 nm (data presented in b).

101

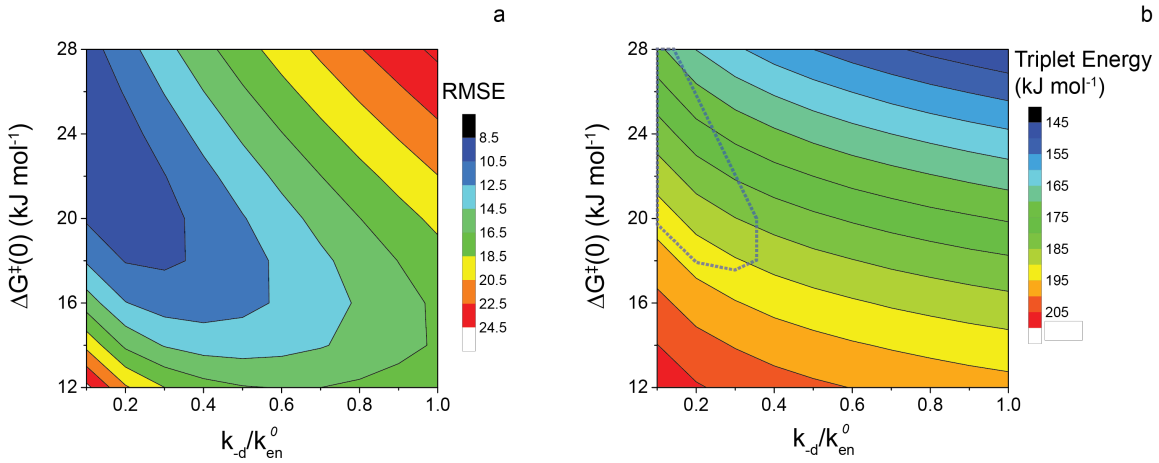

Figure S8 Contour plots showing (a) RMSE of fits and (b) calculated triplet energy based on the parameters $\Delta G^{\ddagger}(0)$ and k_{-d}/k^0_{en} used to fit the quenching of model sensitizer triplets by HDA with eq. 1. The dashed-line in panel b represents the parameter range that yielded RMSE less than 10.5 that was used to calculate the average triplet energy of HDA.

102

103

Section 4. Sorbic Acid Quenching of Model Sensitizer Triplets

Screening Factor for CBBP/PN Sensitizer Mixture

A screening factor (S_λ) was applied to the unquenchable $^1O_2$ phosphorescence signal area produced by the CBBP/PN mixture to account for light screening by CBBP using eq. S8:

$$S_\lambda = \frac{1-10^{-l\times\alpha_\lambda}}{2.303\times l\times\alpha_\lambda} \qquad \text{S8}$$

where α_λ is the solution absorbance (cm^{-1}) and l the experimental path length (cm).

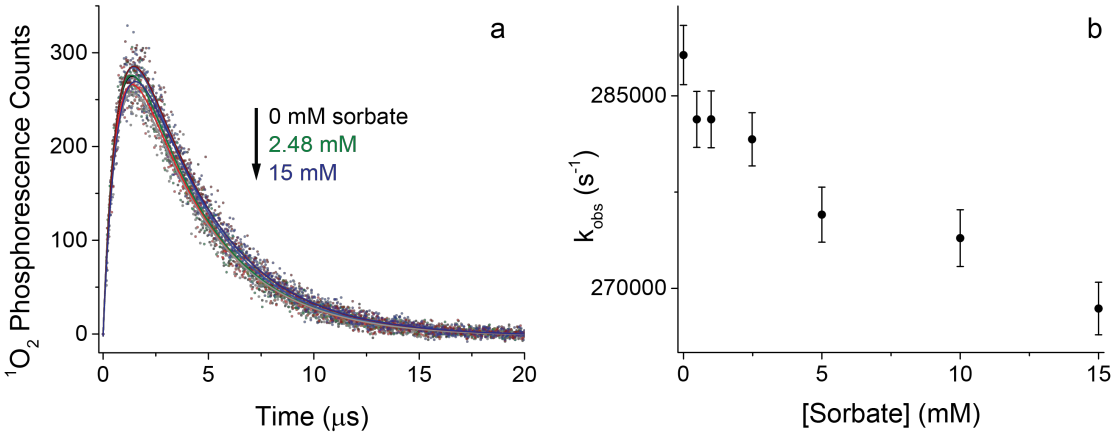

Figure S9 (a) Time-resolved $^1O_2$ phosphorescence traces for ZnTMPyP (λ_{ex} = 450 nm) as a function of added HDA. Solid lines are the generic biexponential kinetic fits described in the text. (b) Decay rate constants of the biexponential fits in panel a, plotted as a function of [HDA].

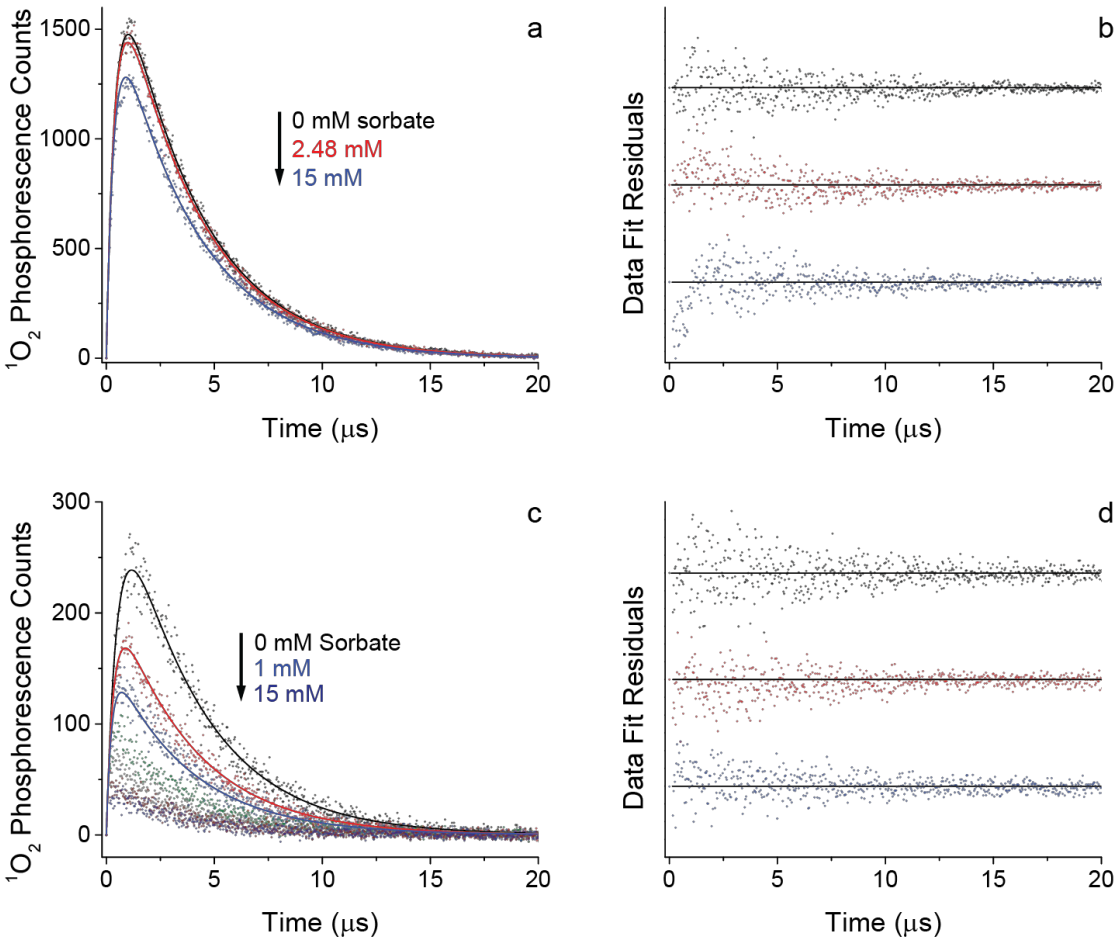

Figure S10 Time-resolved $^1O_2$ phosphorescence traces for (a) PN (λ_{ex} = 340 nm) and (c) CBBP (λ_{ex} = 340 nm) as a function of added HDA. Solid lines are the global kinetic fits as described in the text with associated residuals – displayed adjacent to the fits – in panels b and d.

115

116

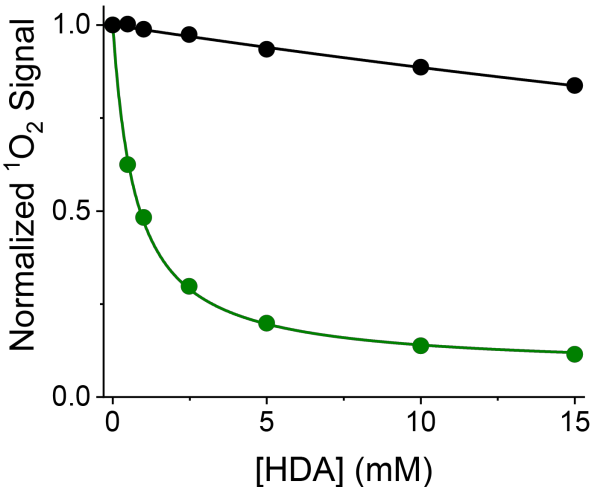

Figure S11 Normalized $^1O_2$ phosphorescence signal areas as a function of added HDA for PN (black) and CBBP (green). Solid lines are the inverse first order fits described in the text.

117

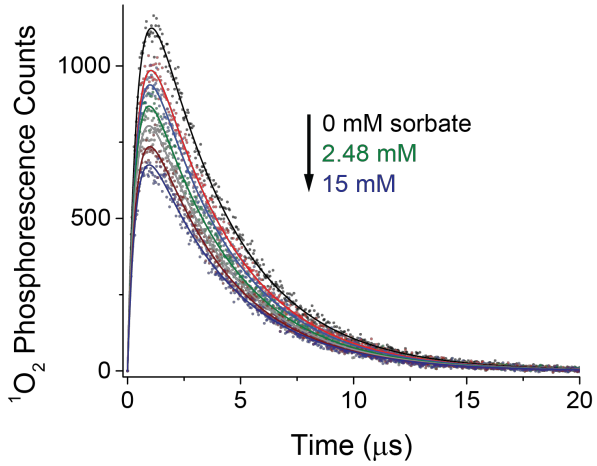

Figure S12 Time-resolved $^1O_2$ phosphorescence traces for CBBP/ PN mixture (λ_{ex} = 340 nm) as a function of added HDA. Solid lines are the generic biexponential kinetic fits described in the text.

118

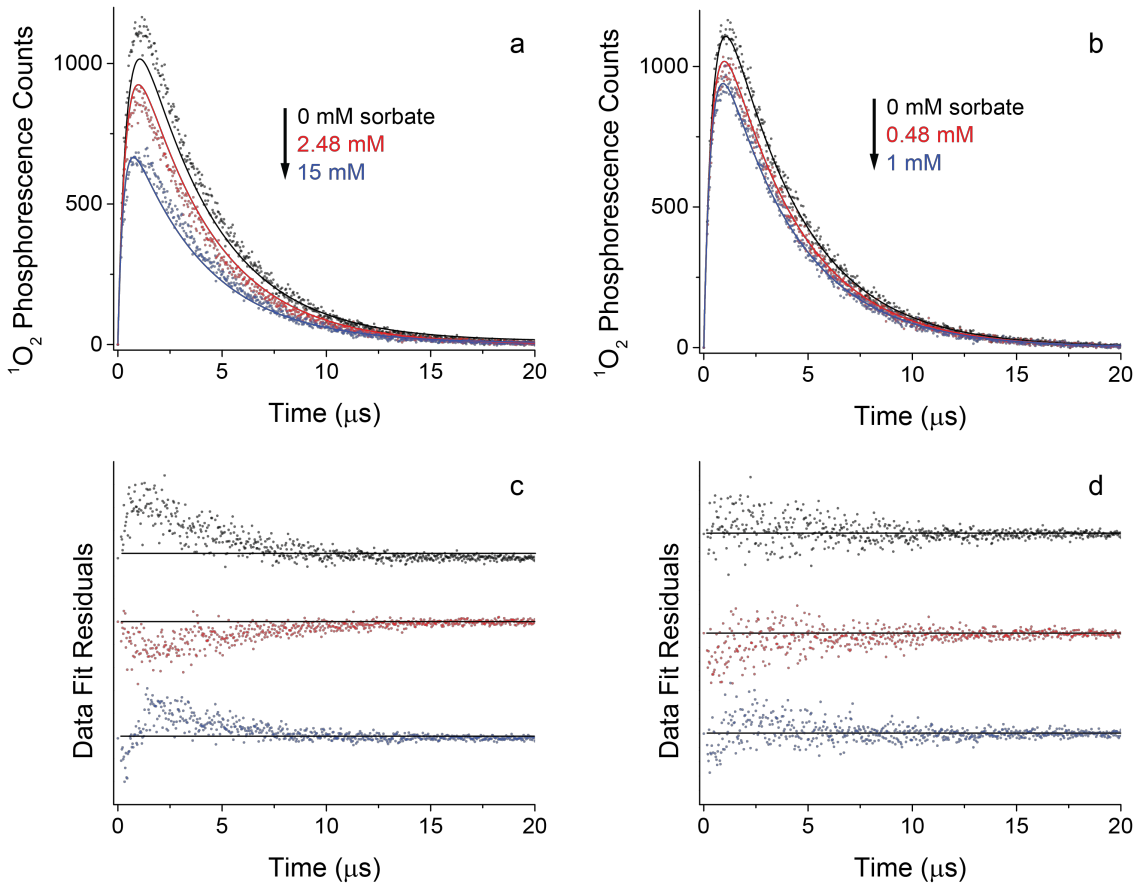

Figure S13 Time-resolved $^1O_2$ phosphorescence traces for CBBP/PN mixture (λ_{ex} = 340 nm) as a function of added HDA fit at (a) high and (b) low [HDA]. Solid lines are the global kinetic fits described in the text. Residuals of global kinetic fits at (c) high and (d) low [HDA].

119

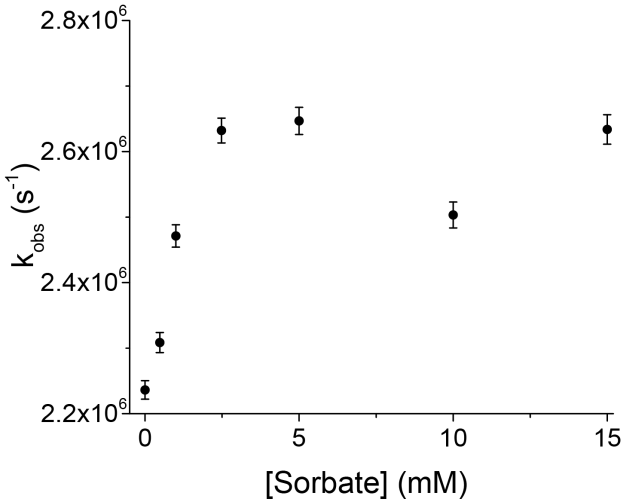

Figure S14 $^1O_2$ phosphorescence growth rate constant (k_{obs}) produced by CBBP/ PN mixture (λ_{ex} = 340 nm) as a function of HDA quencher. k_{obs} was calculated using a generic growth and decay equation.

Section 5. Sorbic Acid Quenching of ^{3}CDOM*

Reproducibility of Quenching Experiments

Reproducibility of the measured rate constants was assessed by repeating HDA quenching experiments of MRNOM in triplicate. The resulting values were quite similar (3.0 ±0.1, 2.8 ±0.1, and 2.8 ±0.1 $\times 10^8$ M^{-1} s^{-1}) with a standard deviation of less than 5% between the values.

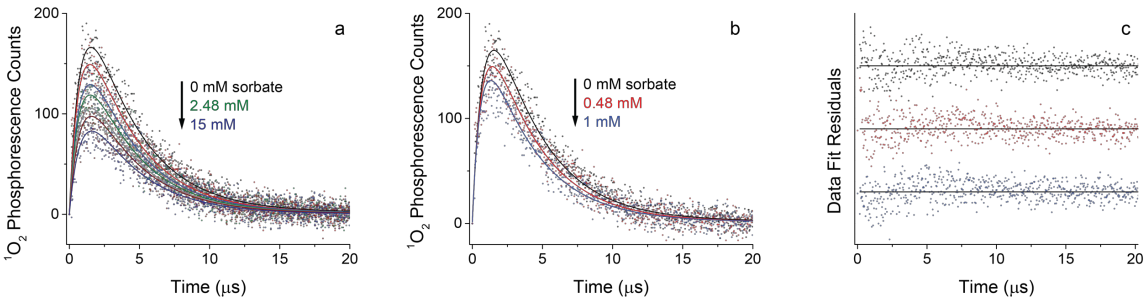

Figure S15 Time-resolved $^1O_2$ phosphorescence traces for SRNOM as a function of added HDA with (a) generic biexponential growth and decay and (b) global kinetic fitting. (c) Residuals of global kinetic fits from associated traces in panel b.

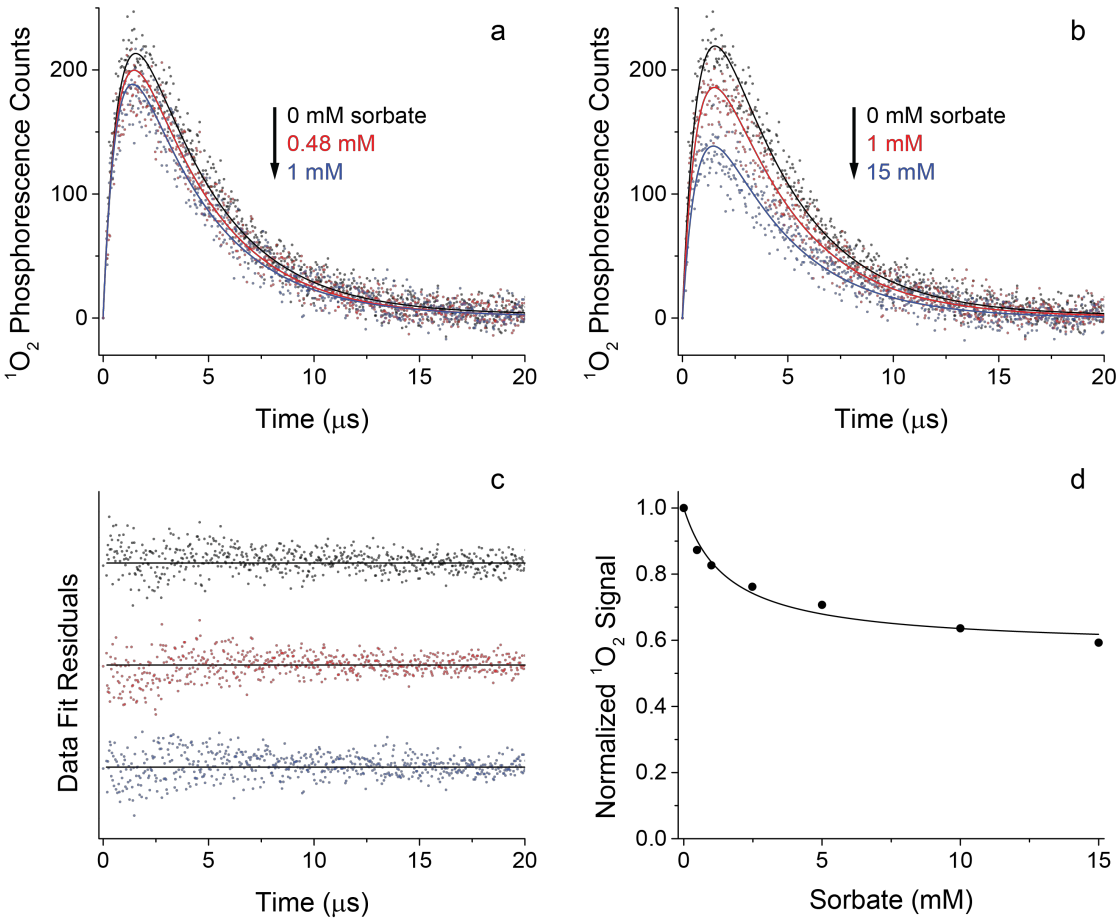

Figure S16 Time-resolved $^1O_2$ phosphorescence traces for SRFA as a function of added HDA with (a) global kinetic and (b) generic biexponential growth and decay fitting. (c) Residuals of global kinetic fits from associated traces in panel a. (d) Normalized $^1O_2$ phosphorescence signal area as a function of added HDA from data in panel b. Solid line is the inverse first order fit.

141

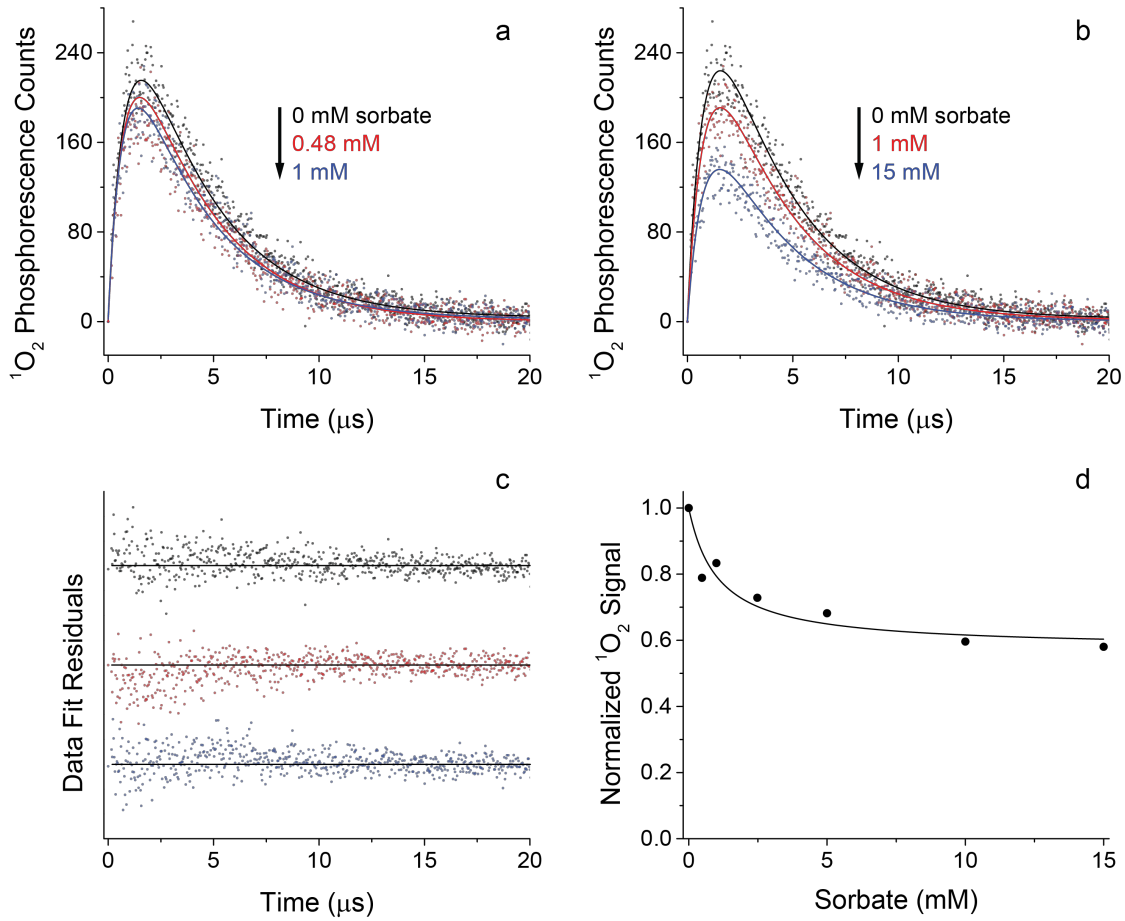

Figure S17 Time-resolved $^1O_2$ phosphorescence traces for Great Dismal Swamp whole water as a function of added HDA with (a) global kinetic and (b) generic biexponential growth and decay fitting. (c) Residuals of global kinetic fits from associated traces in panel a. (d) Normalized $^1O_2$ phosphorescence signal area as a function of added HDA from data in panel b. Solid line is the inverse first order fit.

142

143

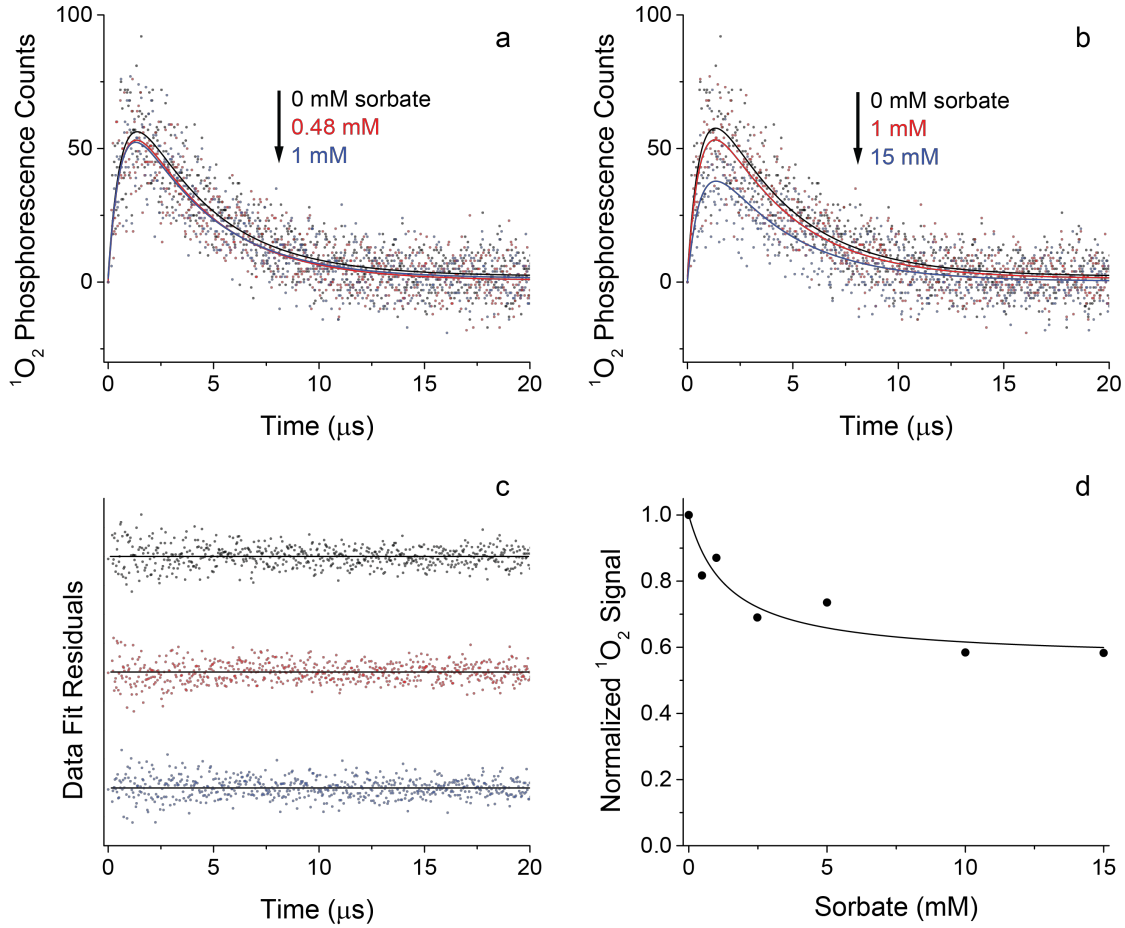

Figure S18 Time-resolved $^1O_2$ phosphorescence traces for SRHA as a function of added HDA with (a) global kinetic and (b) generic biexponential growth and decay fitting. (c) Residuals of global kinetic fits from associated traces in panel a. (d) Normalized $^1O_2$ phosphorescence signal area as a function of added HDA from data in panel b. Solid line is the inverse first order fit.

144

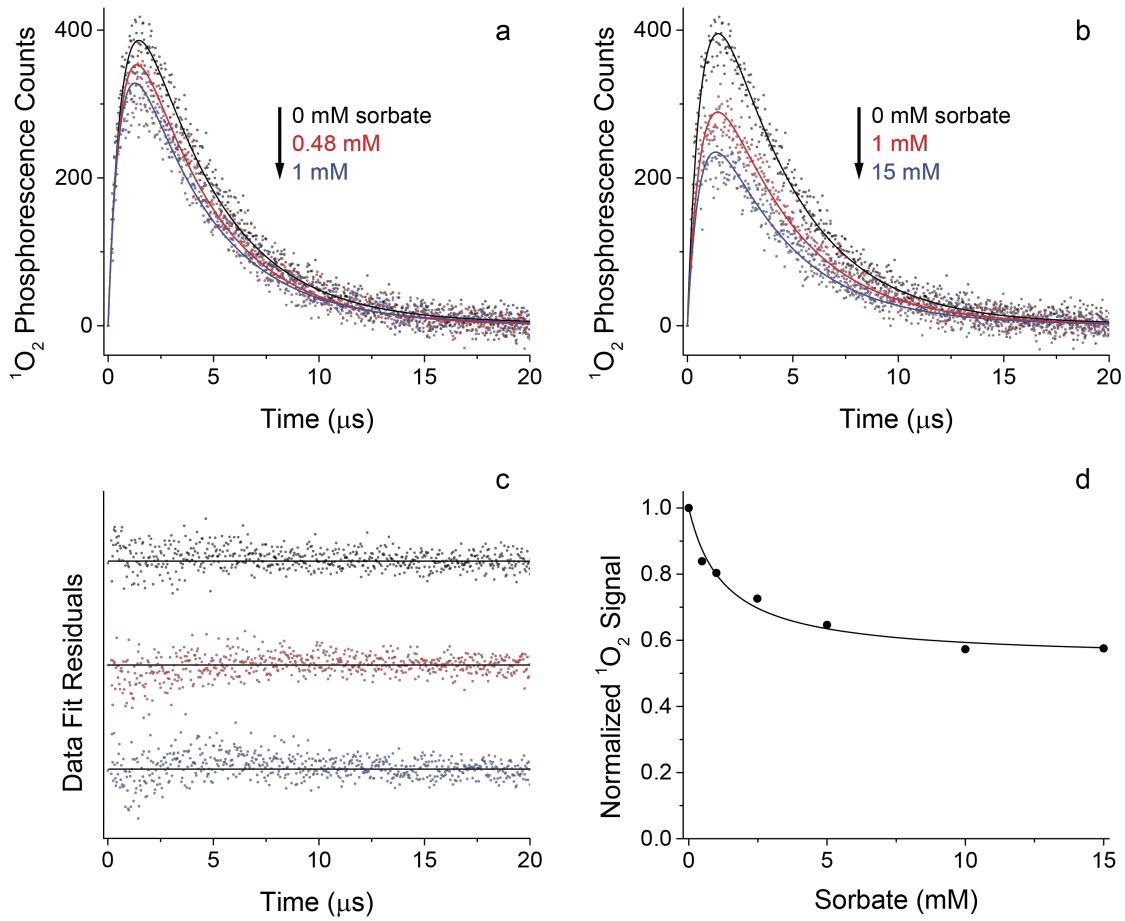

Figure S19 Time-resolved $^1O_2$ phosphorescence traces for Nordic Lake NOM as a function of added HDA with (a) global kinetic and (b) generic biexponential growth and decay fitting. (c) Residuals of global kinetic fits from associated traces in panel a. (d) Normalized $^1O_2$ phosphorescence signal area as a function of added HDA from data in panel b. Solid line is the inverse first order fit.

145

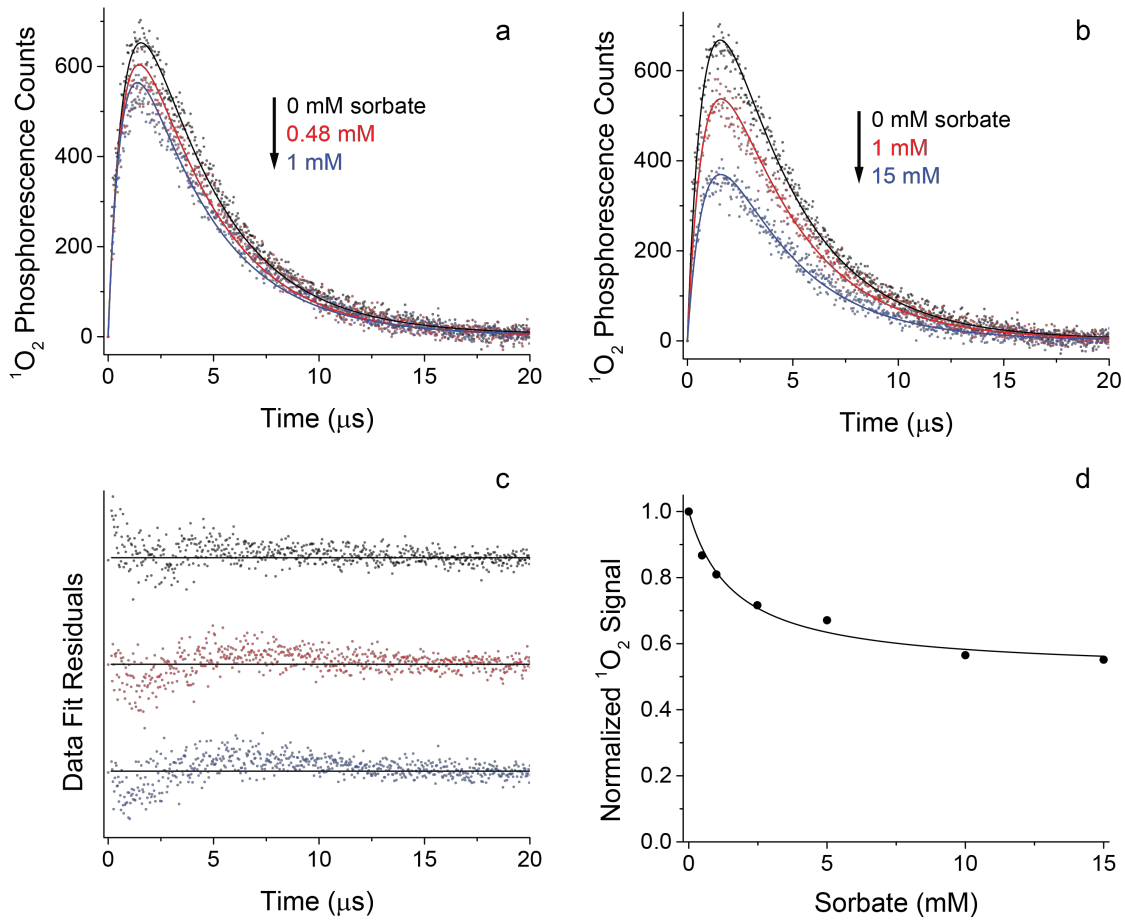

Figure S20 Time-resolved $^1O_2$ phosphorescence traces for Everglades TPIA as a function of added HDA with (a) global kinetic and (b) generic biexponential growth and decay fitting. (c) Residuals of global kinetic fits from associated traces in panel a. (d) Normalized $^1O_2$ phosphorescence signal area as a function of added HDA from data in panel b. Solid line is the inverse first order fit.

146

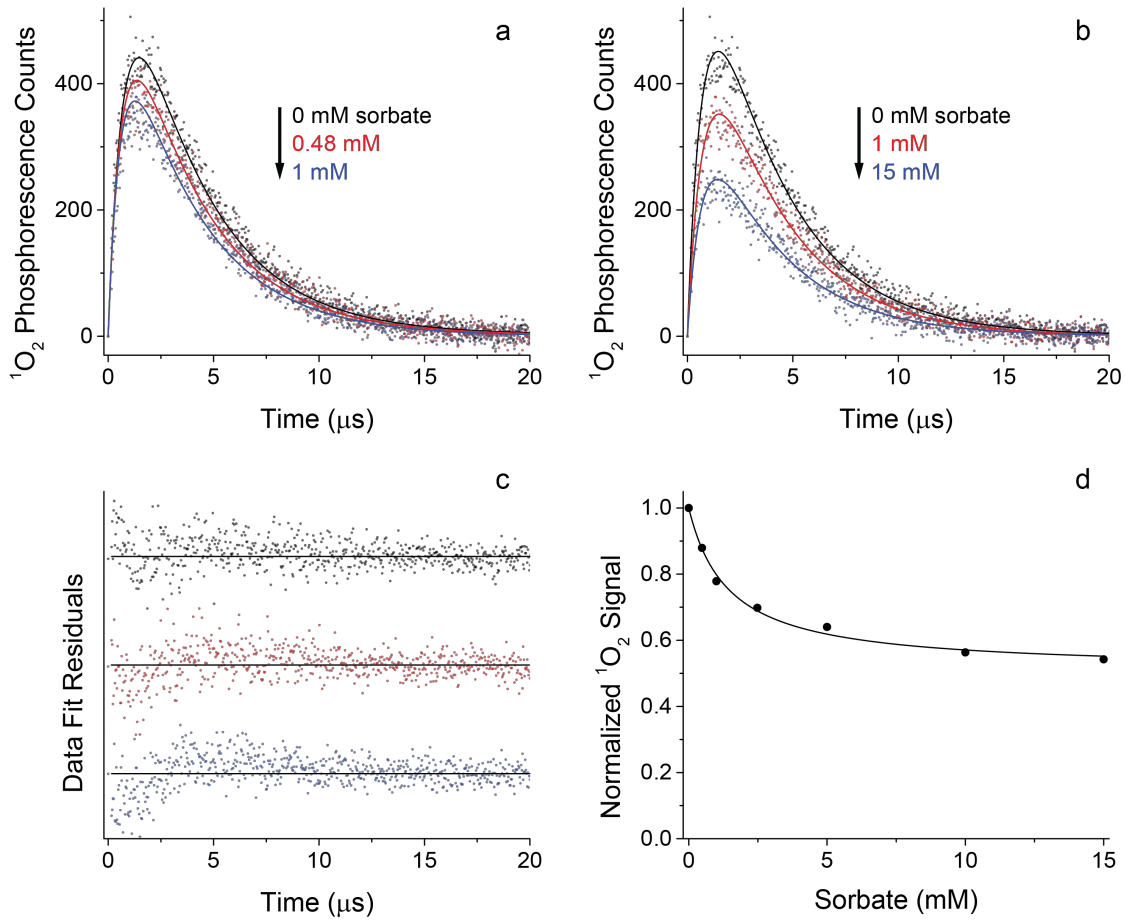

Figure S21 Time-resolved $^1O_2$ phosphorescence traces for Everglades HPOA as a function of added HDA with (a) global kinetic and (b) generic biexponential growth and decay fitting. (c) Residuals of global kinetic fits from associated traces in panel a. (d) Normalized $^1O_2$ phosphorescence signal area as a function of added HDA from data in panel b. Solid line is the inverse first order fit.

147

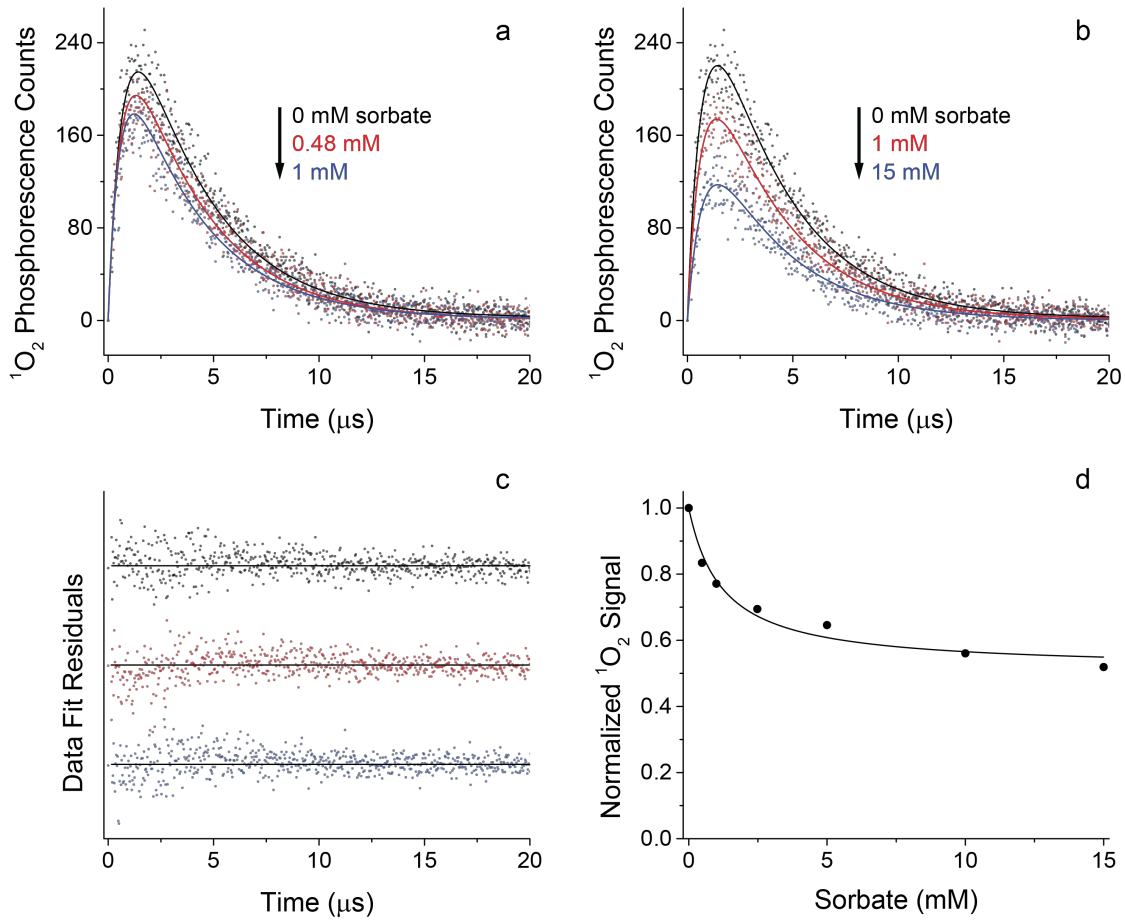

Figure S22 Time-resolved $^1O_2$ phosphorescence traces for Lake Bradford whole water as a function of added HDA with (a) global kinetic and (b) generic biexponential growth and decay fitting. (c) Residuals of global kinetic fits from associated traces in panel a. (d) Normalized $^1O_2$ phosphorescence signal area as a function of added HDA from data in panel b. Solid line is the inverse first order fit.

148

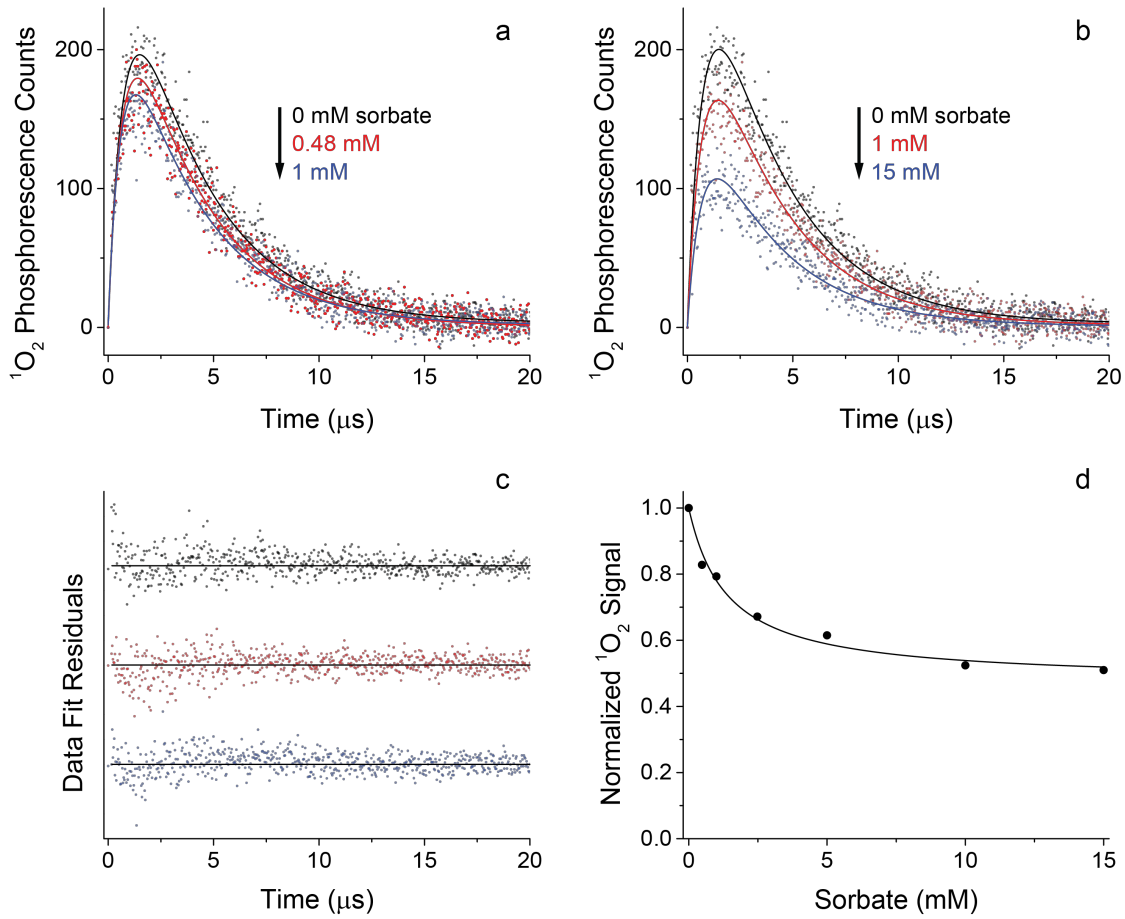

Figure S23 Time-resolved $^1O_2$ phosphorescence traces for Mississippi River NOM as a function of added HDA with (a) global kinetic and (b) generic biexponential growth and decay fitting. (c) Residuals of global kinetic fits from associated traces in panel a. (d) Normalized $^1O_2$ phosphorescence signal area as a function of added HDA from data in panel b. Solid line is the inverse first order fit.

149

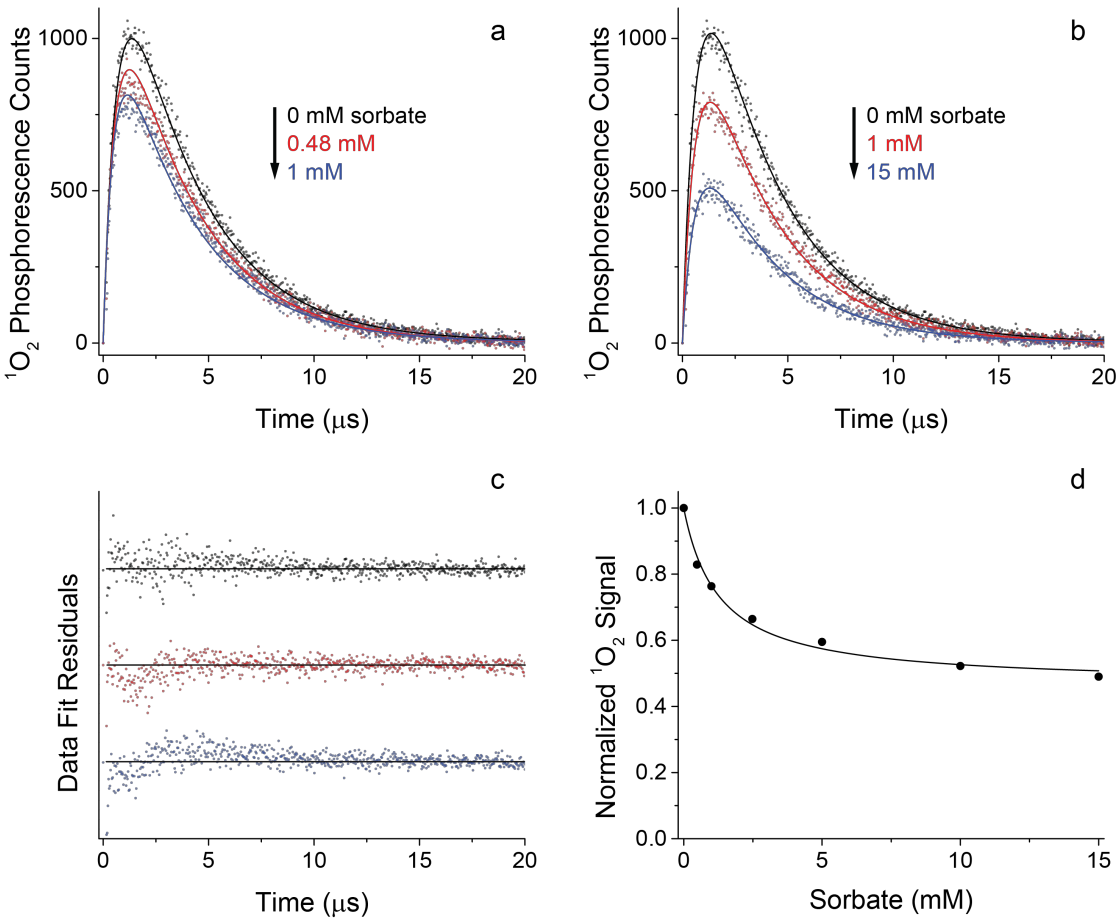

Figure S24 Time-resolved $^1O_2$ phosphorescence traces for Everglades HPON as a function of added HDA with (a) global kinetic and (b) generic biexponential growth and decay fitting. (c) Residuals of global kinetic fits from associated traces in panel a. (d) Normalized $^1O_2$ phosphorescence signal area as a function of added HDA from data in panel b. Solid line is the inverse first order fit.

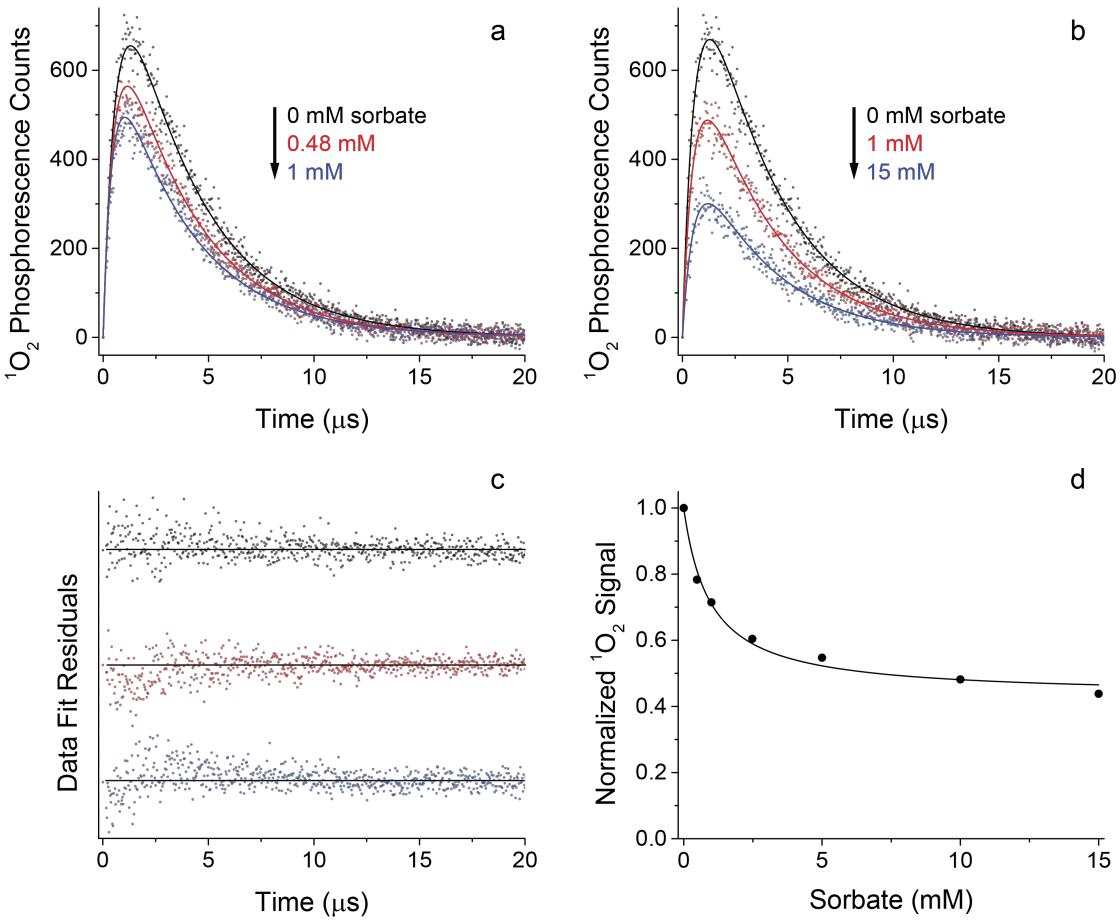

Figure S25 Time-resolved $^1O_2$ phosphorescence traces for Williams Lake HPON as a function of added HDA with (a) global kinetic and (b) generic biexponential growth and decay fitting. (c) Residuals of global kinetic fits from associated traces in panel a. (d) Normalized $^1O_2$ phosphorescence signal area as a function of added HDA from data in panel b. Solid line is the inverse first order fit.

151

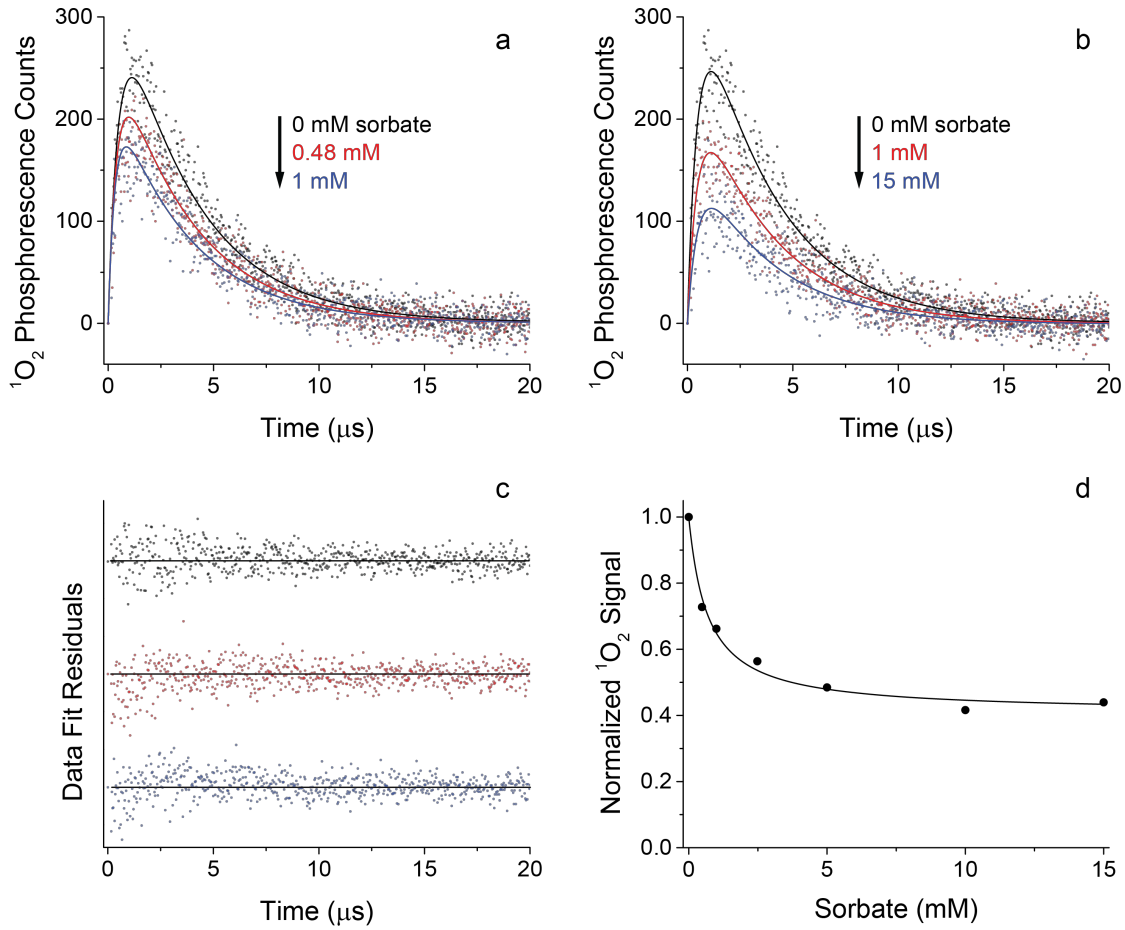

Figure S26 Time-resolved $^1O_2$ phosphorescence traces for Pacific Ocean HPOA as a function of added HDA with (a) global kinetic and (b) generic biexponential growth and decay fitting. (c) Residuals of global kinetic fits from associated traces in panel a. (d) Normalized $^1O_2$ phosphorescence signal area as a function of added HDA from data in panel b. Solid line is the inverse first order fit.

152

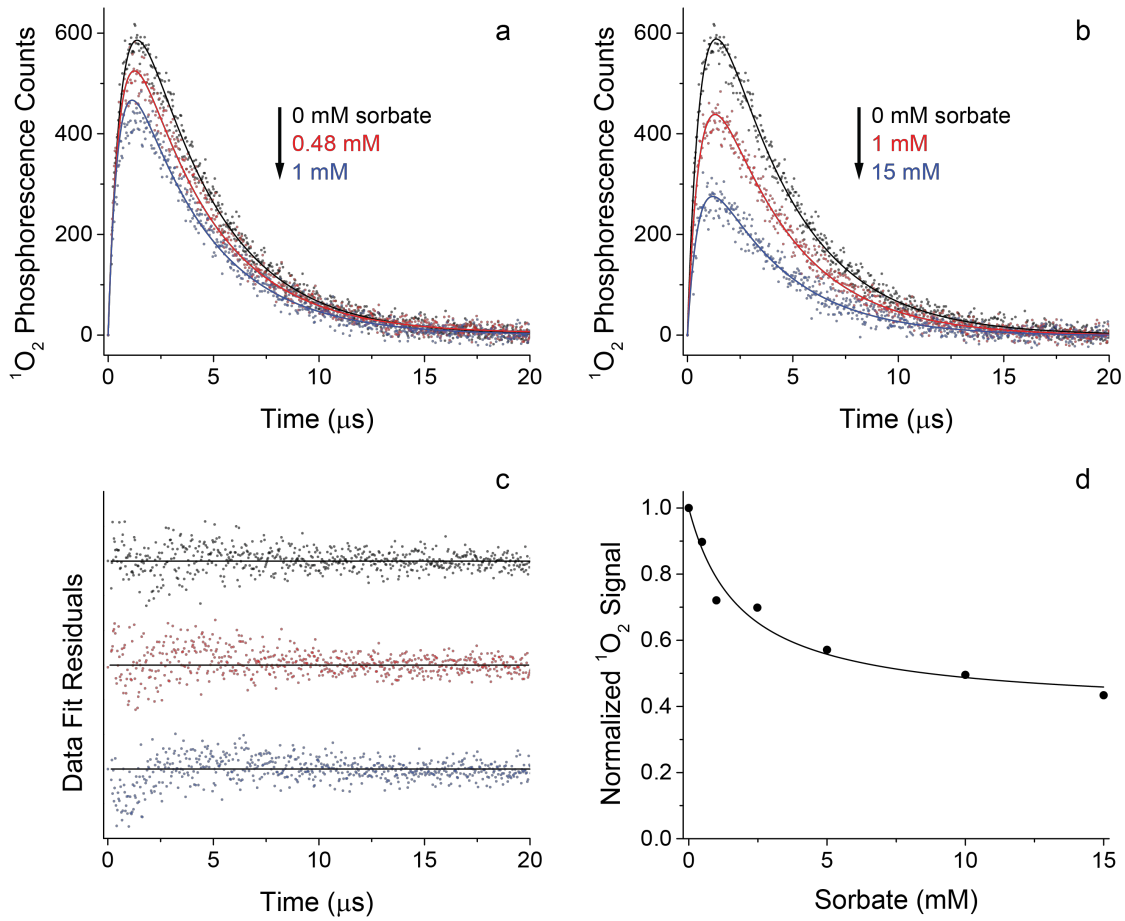

Figure S27 Time-resolved $^1O_2$ phosphorescence traces for Williams Lake HPOA as a function of added HDA with (a) global kinetic and (b) generic biexponential growth and decay fitting. (c) Residuals of global kinetic fits from associated traces in panel a. (d) Normalized $^1O_2$ phosphorescence signal area as a function of added HDA from data in panel b. Solid line is the inverse first order fit.

153

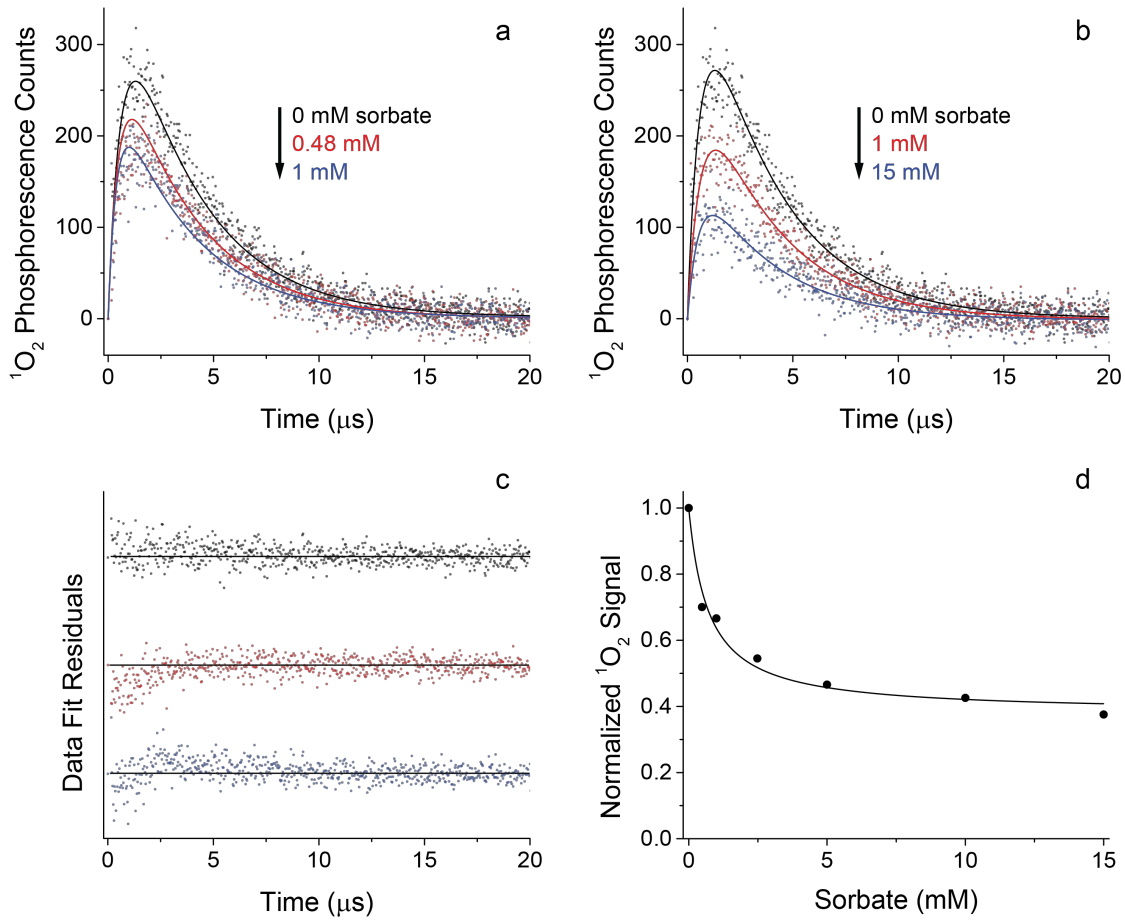

Figure S28 Time-resolved $^1O_2$ phosphorescence traces for Williams Lake TPIA as a function of added HDA with (a) global kinetic and (b) generic biexponential growth and decay fitting. (c) Residuals of global kinetic fits from associated traces in panel a. (d) Normalized $^1O_2$ phosphorescence signal area as a function of added HDA from data in panel b. Solid line is the inverse first order fit.

154

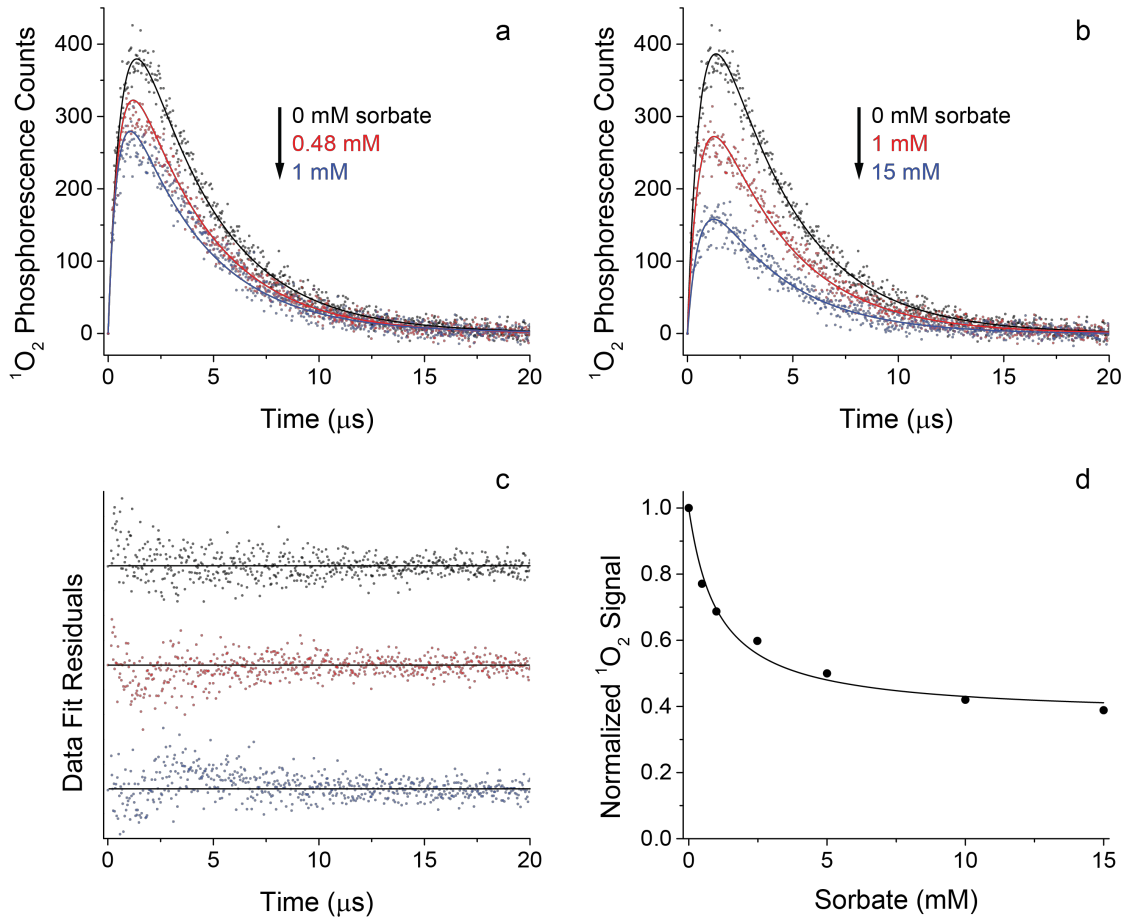

Figure S29 Time-resolved $^1O_2$ phosphorescence traces for Pony Lake FA as a function of added HDA with (a) global kinetic and (b) generic biexponential growth and decay fitting. (c) Residuals of global kinetic fits from associated traces in panel a. (d) Normalized $^1O_2$ phosphorescence signal area as a function of added HDA from data in panel b. Solid line is the inverse first order fit.

155

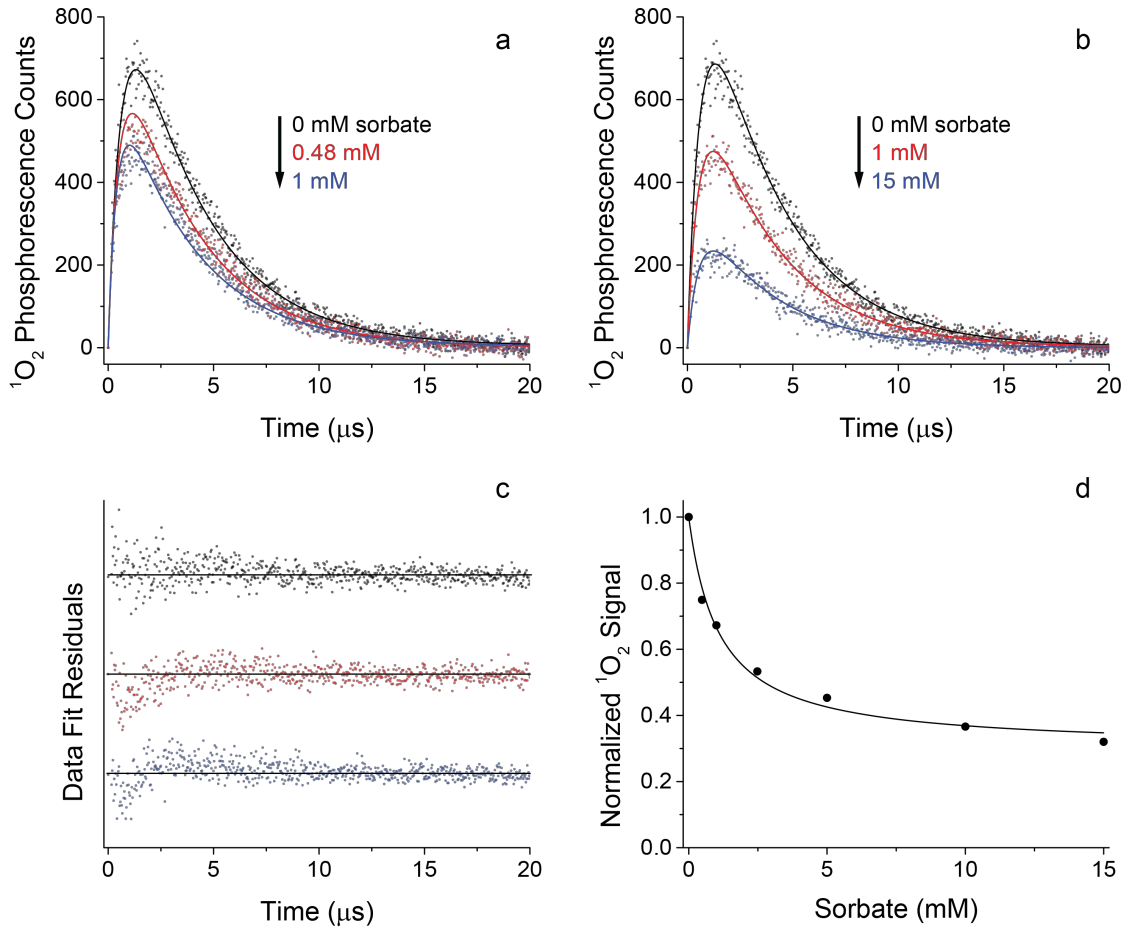

Figure S30 Time-resolved $^1O_2$ phosphorescence traces for Lake Fryxell FA as a function of added HDA with (a) global kinetic and (b) generic biexponential growth and decay fitting. (c) Residuals of global kinetic fits from associated traces in panel a. (d) Normalized $^1O_2$ phosphorescence signal area as a function of added HDA from data in panel b. Solid line is the inverse first order fit.

156

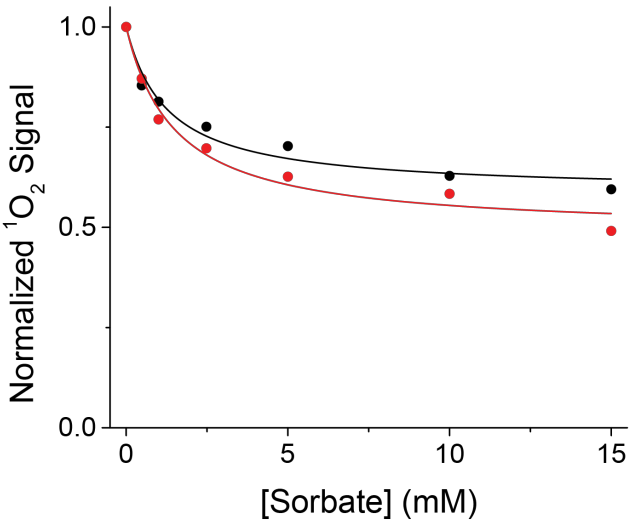

Figure S31 Normalized $^1O_2$ phosphorescence signal area as a function of added HDA for SRNOM in methanol (black) and water (red). Solid lines are the inverse first order fits.

157

158

Section 6. Comparing k_{HDA} from Single Pool and Two-Pool Fitting Approaches

To compare k_{HDA} values determined from the single pool and two-pool fitting approaches, a k_{HDA} value for all triplets in CDOM (k_{AVG}) was calculated using eq. S9:

$$k_{AVG} = \alpha_{low} k_{low} + (1 - \alpha_{low}) k_{high} \quad \text{S9}$$

where α_{low} is the unquenchable fraction determined from the two-pool fitting approach, k_{low} is k_{HDA} for the low energy triplet pool (assumed to equal 0), and k_{high} is k_{HDA} for the high energy triplet pool determined from the two-pool fitting approach. Calculated k_{AVG} values are compared to k_{HDA} values determined with the single pool fitting approach in Table S3.

Table S3 Rate constants of HDA quenching of ^{3}CDOM* for various DOM sources determined with eq. S8 (k_{AVG}) and global kinetic fitting (k_{HDA}).

DOM	k_{AVG} (10^8 M^{-1} s^{-1})	k_{HDA} (10^8 M^{-1} s^{-1}) Global Kinetic
Suwannee River FA	3.4 (±0.8)	2.2 (±0.1)
Great Dismal Swamp	5.0 (±2.0)	2.1 (±0.1)
Suwannee River HA	4.9 (±2.4)	1.2 (±0.4)
Nordic Lake NOM	5.0 (±1.0)	3.3 (±0.1)
Everglades TPIA	3.7 (±0.7)	2.6 (±0.1)
Everglades HPOA	4.7 (±0.7)	3.3 (±0.1)
Lake Bradford	5.7 (±1.3)	3.8 (±0.1)
Mississippi River NOM	3.7 (±0.9)	2.9 (±0.1)
Suwannee River NOM	4.3 (±1.0)	3.6 (±0.1)
Everglades HPON	6.4 (±1.0)	4.6 (±0.1)

Williams Lake HPON	9.9 (±1.6)	7.2 (±0.1)
Pacific Ocean HPOA	17.9 (±3.0)	10.2 (±0.3)
Williams Lake HPOA	4.9 (±1.3)	5.3 (±0.1)
Williams Lake TPIA	14.5 (±3.0)	8.2 (±0.2)
Pony Lake FA	9.2 (±1.6)	7.4 (±0.1)
Lake Fryxell FA	10.4 (±1.6)	8.0 (±0.1)

171

172

173

174

175

176

177

Section 7. Past Estimates of Triplet Distribution in CDOM

Table S4 Data from Zepp et al.[7] updated using an assumed f_Δ value of 0.95 and a revised k_{O_2} value for ^{3}CDOM*(9×10^8 M^{-1} s^{-1}),[1, 8] which affects the calculation of [^{3}CDOM*] > 94 kJ mol^{-1} and thus impacts α.

Water Sample	[$^1O_2$] (10^{-13} M)	[^{3}CDOM*] > 94 kJ mol^{-1} (10^{-13} M)	[^{3}CDOM*] > 250 kJ mol^{-1} (10^{-13} M)	α
Aucilla River	4.4	5.7	1.0	0.82
Suwannee River	4.1	5.3	0.7	0.87
Wylde Lake humus	2.5	3.2	0.4	0.89
Ohio River fulvic acid	9.4	12.1	1.8	0.85
Fluka AG humic acid	4.1	5.3	0.3	0.94
Aldrich humic acid	3.8	4.9	1.0	0.80
Contech fulvic acid	3.8	4.9	0.6	0.88

References

1. Erickson, P. R.; Moor, K. J.; Werner, J. J.; Latch, D. E.; Arnold, W. A.; McNeill, K., Singlet Oxygen Phosphorescence as a Probe for Triplet-State Dissolved Organic Matter Reactivity. *Environmental Science & Technology* **2018,** *52*, (16), 9170-9178.
2. Appiani, E.; Ossola, R.; Latch, D.; Erickson, P. R.; McNeill, K., Aqueous singlet oxygen reaction kinetics of furfuryl alcohol: Effect of temperature, pH, and salt content. *Environmental Science: Processes & Impacts* **2017,** *19*, (4), 507-516.
3. Wenk, J.; Eustis, S. N.; McNeill, K.; Canonica, S., Quenching of Excited Triplet States by Dissolved Natural Organic Matter. *Environmental Science & Technology* **2013,** *47*, (22), 12802-12810.
4. Canonica, S.; Hellrung, B.; Wirz, J., Oxidation of Phenols by Triplet Aromatic Ketones in Aqueous Solution. *The Journal of Physical Chemistry A* **2000,** *104*, (6), 1226-1232.
5. McNeill, K.; Canonica, S., Triplet state dissolved organic matter in aquatic photochemistry: reaction mechanisms, substrate scope, and photophysical properties. *Environmental Science: Processes & Impacts* **2016,** *18*, (11), 1381-1399.
6. Flors, C.; Nonell, S., On the Phosphorescence of 1H-Phenalen-1-one. *Helvetica Chimica Acta* **2001,** *84*, (9), 2533-2539.
7. Zepp, R. G.; Schlotzhauer, P. F.; Sink, R. M., Photosensitized transformations involving electronic energy transfer in natural waters: role of humic substances. *Environmental Science & Technology* **1985,** *19*, (1), 74-81.

202 8. Zhou, H.; Yan, S.; Lian, L.; Song, W., Triplet-State Photochemistry of
203 Dissolved Organic Matter: Triplet-State Energy Distribution and Surface Electric
204 Charge Conditions. *Environmental Science & Technology* **2019,** *53*, (5), 2482-2490.
205